Advantage of the Mark-III FEL for biophysical research and biomedical applications†

Glenn S. Edwards* and M. Shane Hutson

Duke University Free Electron Laser Laboratory, Durham, NC 27708, USA. E-mail: edwards@fel.duke.edu

Although 6.45 µm is not the strongest absorption band of biological tissues in the mid-infrared, a Mark-III free-electron laser (FEL) tuned to this wavelength can efficiently ablate tissue while minimizing collateral damage. A model has previously been presented that explains this wavelength dependence as a competition between two dynamic processes – explosive vaporization of saline and denaturation of structural proteins. Here it is shown that this model predicts a 'sweet-spot' for each wavelength, *i.e.* a region of parameter space (incident intensity and pulse width) in which explosive vaporization is preceded by substantial protein denaturation. This sweet-spot is much larger for wavelengths where protein is the dominant chromophore. At other wavelengths, collateral damage may be minimized within the sweet-spot, but the maximum intensities and pulse widths in these regions are insufficient to remove tissue at surgically relevant rates.

1. Introduction

The goals of surgical laser ablation are twofold: to remove a defined volume of tissue at a substantial rate, and to leave the adjacent tissue biologically viable. These goals can be attained using a mid-infrared Mark-III free-electron laser (FEL) tuned to wavelengths near 6.45 µm, where such FELs are operational at Duke and Vanderbilt Universities (Colson *et al.*, 2002). Although 6.45 µm does not coincide with the strongest absorption band in the mid-infrared spectra of soft biological tissues, previous experiments have shown that FEL radiation at this wavelength is superior for surgical applications (Edwards *et al.*, 1994). In fact, a Mark-III FEL has been used in human neurosurgery (Copeland *et al.*, 1998, 2000) and ophthalmic procedures (Joos *et al.*, 2000) with successful outcomes.

To account for this wavelength-dependence, a thermodynamic model was proposed (Edwards *et al.*, 1994). Wavelengths near 6.45 µm couple energy into two broad spectral features: the bending mode of water centered at 6.1 µm and the amide-II vibrational mode of proteins centered at 6.45 µm. The stronger infrared absorption bands of tissue couple predominantly into water modes. Thus, thermodynamic reasoning suggested that the reduction in collateral damage at 6.45 µm was due to energy partitioning between the protein and saline components of tissues.

We have recently reported a dynamic model that confirms this thermodynamic insight while clarifying the role of the Mark-III FEL superpulse structure (Hutson *et al.*, 2002; Edwards *et al.*, 2002). The Mark-III FEL superpulse consists of a 2–6 µs-long train of picosecond pulses at 2.85 GHz (Madey, 1971). In typical operation, superpulses are repeated at 10–30 Hz. Our dynamic model suggests that the observed wavelength-dependence of Mark-III FEL tissue abla-

tion is not strongly influenced by peak power in the picosecond pulses. Rather, the wavelength-dependence is a consequence of competition between protein denaturation and the explosive vaporization of saline on the 10–100 ns time scale. These dynamic processes are driven by high average power within a superpulse.

Here we expand our model calculations to investigate a broader range of laser intensities and pulse widths. We examine protein and saline dynamics during exposure to radiation at three wavelengths (3.0, 6.1 and 6.45 µm) with comparable protein absorption coefficients, but dramatically different saline absorption coefficients. We show that the model predicts a 'sweet-spot' for each wavelength, *i.e.* a region of parameter space (incident intensity and pulse width) in which explosive vaporization is preceded by substantial protein denaturation. This sweet-spot is much larger at 6.45 µm, where protein is the dominant chromophore. At the other wavelengths, collateral damage may be minimized within the sweet-spot, but the maximum intensities and pulse widths in these regions are insufficient to remove tissue at surgically relevant rates.

2. Methods

Spectra of porcine corneal stroma and saline were measured on a Bruker IFS-66 FTIR spectrometer with a ZnSe single-bounce ATR crystal. Before further processing, spectra were corrected for the $1/\lambda$ dependence in the sampling depth of the evanescent wave. To generate the protein component spectrum, we interactively subtracted the saline spectrum from the stroma spectrum to minimize the water association band centered at 4.7 µm. The measured saline spectrum was scaled by the coefficient determined in the subtraction procedure to generate the saline component spectrum. To find the component absorption coefficients, both component spectra were scaled so that the 6.1 µm peak of the saline spectrum corresponded to an absorption coefficient of 0.27 µm^{-1} (Hale & Querry, 1973).

We model corneal stroma as 30 nm alternating layers of protein and saline (Davson, 1972). This is an idealization, ignoring saline retained within the protein layer. We performed calculations to simulate laser heating and thermal diffusion in this model as previously described (Hutson *et al.*, 2002; Edwards *et al.*, 2002). Briefly, thermal diffusion is described by Fourier's equation, where laser heating of the medium is accounted for by an additional source term Q, to yield the heat balance equation (Landau & Liftshitz, 1987),

$$\rho c_p \frac{\partial T}{\partial t} = \kappa \Delta T + Q, \tag{1}$$

where ρ is the density, c_p is the specific heat at constant pressure, T is the temperature and κ is the thermal conductivity. We apply the heat balance equation to our laminar system. The protein has the optical and thermal properties of collagen, and both air and saline are characterized by their own distinctive optical and thermal properties (Edwards *et al.*, 1994; Kampmeier *et al.*, 2000). The penetration depths used to model protein and saline absorption of the incident radiation are given in Table 1. Protein denaturation during laser

Table 1
Penetration depths of corneal stroma, as well as its saline and protein components.

	Penetration depth (µm)		
	$\lambda = 3.0$ µm	$\lambda = 6.1$ µm	$\lambda = 6.45$ µm
Saline	1.0	3.7	12.0
Protein	10.0	8.0	8.0
Stroma	1.8	5.1	9.6

---

† Presented at the 'XIV Russian Synchrotron Radiation Conference SR2002', held at Novosibirsk, Russia, on 15–19 July 2002.
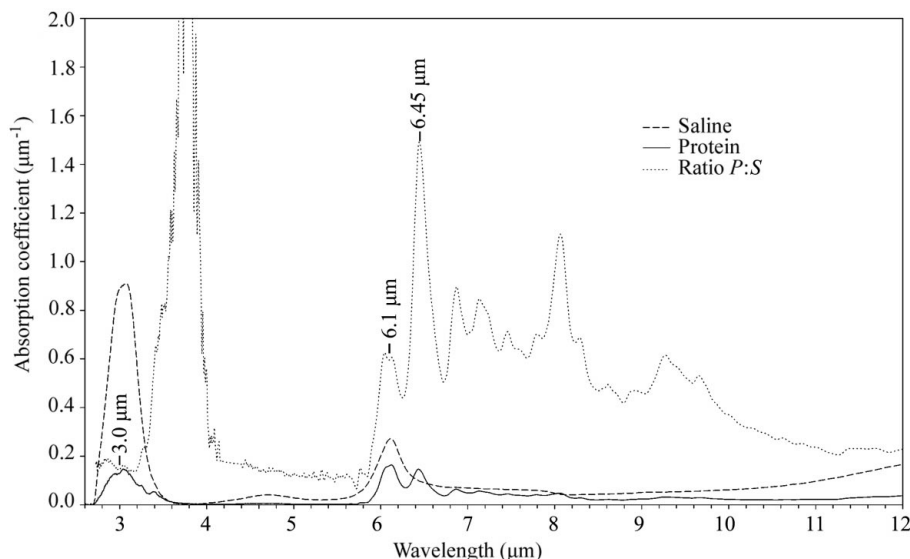
Figure 1
Mid-IR spectra of the saline (dashed line) and protein (solid line) components of corneal stroma. The spectra have been scaled so that the absorption coefficient for saline at 6.1 µm is 0.27 µm^{-1} (Hale & Querry, 1973). Although the protein absorption coefficients are similar at 3.0, 6.1 and 6.45 µm, the protein-to-saline ratios of the absorption coefficients (dots) differ dramatically.

heating was estimated by an Arrhenius formulation of first-order kinetics (Kampmeier *et al.*, 2000),

$$\frac{1}{C}\frac{dC}{dt} = \frac{RT(t)}{hN_a}\exp(1 + \Delta S^*/R)\exp[-E^*/RT(t)], \qquad (2)$$

where E^* (106 kJ mol^{-1}) is the activation energy and ΔS^* (39 J mol^{-1} K^{-1}) is the activation entropy. Explosive vaporization of saline was treated as a threshold event at the superheat limit of saline, 575 K (Skripov, 1988).

3. Results and discussion

Absorption coefficients for the protein and saline components of corneal stroma are shown in Fig. 1. The locations of the three strongest mid-infrared absorptions of stroma are specifically marked at 3.0, 6.1 and 6.45 µm. Each wavelength overlaps both protein and saline spectral features: 3.0 µm overlaps the very strong OH stretch mode of water and the amide NH stretch mode of proteins; 6.1 µm overlaps the strong bending mode of water and the amide-I mode of proteins; and 6.45 µm overlaps the long-wavelength wing of the water bending mode as well as the amide-II mode of proteins. Taking the inverse of the absorption coefficients gives the penetration depths listed in Table 1. Although the penetration depth for protein is comparable at all three wavelengths, it is clear from the absorption ratio shown in Fig. 1 that much more energy is partitioned into the protein component of stroma at 6.45 µm as compared with either 3.0 or 6.1 µm. In two other regions, 3.8 and 8.1 µm, the absorption ratio is also >1. In the 3.8 µm region, the absorption coefficient ratio exceeds 3, but the coupling of laser radiation into tissue in this spectral range is very weak; at 3.8 µm the penetration depth for stroma is more than 300 µm. The blue side of this region, around 3.4 µm, has a moderate absorption strength and may hold some promise for tissue ablation, likewise for the 8.1 µm region where the penetration depth of stroma is only 23 µm.

As shown for the three wavelengths of interest in Fig. 2, the protein-to-saline absorption ratio has a large effect on the upper limit of superpulse intensity for which collateral damage is minimized. Using our model calculations of the time–temperature history for a

given wavelength and varying superpulse intensities, we compiled the times at which the surface saline layer first reached 575 K. As shown in Fig. 2, these points define the energy density thresholds for explosive vaporization of saline (dashed line) (Venugopalan *et al.*, 1996). Similarly, we compiled the times at which 1% denaturation was reached in the surface protein layer. We take these points to define the threshold for mechanically compromising tissue through the denaturation of structural proteins (solid line). If we redefine the criterion as 0.1% or 10% denaturation, the threshold curves of Fig. 2 only shift by a line width or two. The small magnitude of this shift is due to the exponential dependence of the denaturation rate on temperature in the Arrhenius equation (Kampmeier *et al.*, 2000). To minimize collateral damage, we seek to mechanically compromise the tissue prior to explosive vaporization. This condition is satisfied for superpulse intensities below a wavelength-dependent upper limit. In Fig. 2 this transition is marked by the horizontal dotted line through the point where the 1% denaturation threshold crosses the energy density threshold for explosive vaporization. This limit is only 2.5 × 10^{10} W m^{-2} at 3.0 µm, but increases to 3.0 × 10^{13} W m^{-2} at 6.45 µm. A factor of five in this difference is due to the stronger average absorption at 3.0 µm, but the remainder is due to the higher protein-to-saline absorption ratio at 6.45 µm.

For pulse widths shorter than ∼100 ns the threshold curves are dependent upon the protein-to-saline absorption ratio. Laser heating of a laminar material like corneal stroma leads to layer-specific heating rates. The competition between layer-specific heating rates and thermal diffusion can result in significant temperature differences between adjacent protein and saline layers (Hutson *et al.*, 2002; Edwards *et al.*, 2002). When saline is the predominant chromophore, the temperatures of the saline layers exceed those of the protein layers. This temperature difference pushes the two threshold curves apart – the 1% denaturation curve moves to longer pulse widths while the explosive vaporization curve moves to shorter pulse widths. Thus, the upper limit on superpulse intensity decreases. On the other hand, when protein is the predominant chromophore, the temperatures of the protein layers exceed those of the saline layers. This temperature difference pulls the threshold curves together and increases the upper limit on superpulse intensity. The threshold curves of Fig. 2 can be normalized for average absorption by plotting power density instead of incident intensity. When this is done (not shown), the wavelength-dependence of these power density threshold curves disappears for pulse widths longer than ∼100 ns.

While minimization of collateral damage sets an upper limit on the superpulse intensity, additional limits are imposed by the need to remove tissue through explosive vaporization. First, the laser source must provide enough total energy per superpulse to exceed the energy density threshold for explosive vaporization. We have already calculated this limit (dashed line). Second, the laser source must provide sufficient power density for superheating to occur (dot-dashed line). More specifically, the rate at which energy is deposited into the saline layers must exceed the rate at which energy is consumed by the growth of heterogeneous nuclei, *i.e.* pre-existing vapor phase bubbles (Skripov, 1988; Venugopalan *et al.*, 1996). Under

these conditions the temperature of the saline layers will increase until the onset of homogeneous nucleation of the vapor phase, *i.e.* explosive vaporization. The power density threshold curves shown in Fig. 2 correspond to a heterogeneous nucleating density of 10^{15} m^{-3} (Venugopalan *et al.*, 1996). For a given superpulse intensity, and thus heating rate, superheating will cease for pulse durations longer than the thresholds shown in Fig. 2.
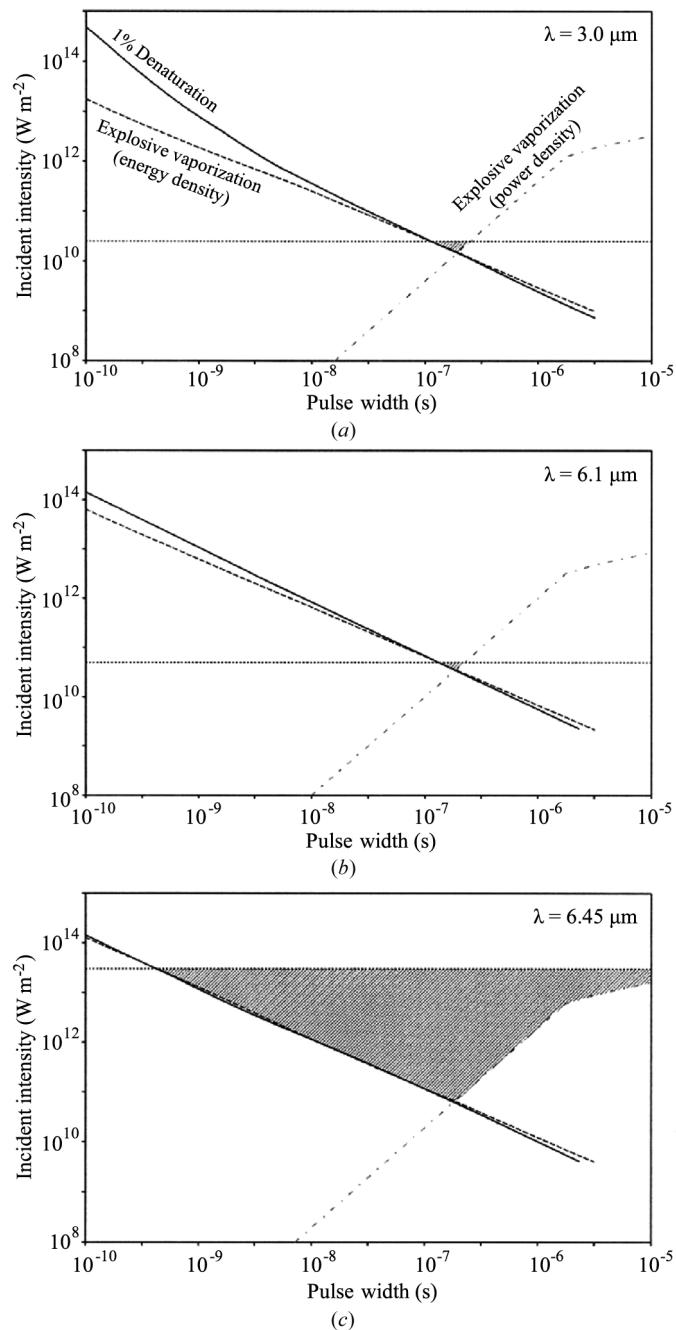

Figure 2
Optimal ranges of intensity and pulse duration (hatched regions) for single-pulse tissue ablation with minimal collateral damage at three infrared wavelengths: (*a*) 3.0 µm, (*b*) 6.1 µm and (*c*) 6.45 µm. To remove tissue by explosive vaporization the exposure conditions must exceed two thresholds: the power density (dot-dashed line) required to heat saline rapidly enough for superheating to occur and the energy density (dashed line) required to reach its superheat limit. To minimize collateral damage the incident intensity must fall below the threshold (dots) at which 1% denaturation of the protein (solid line) precedes explosive vaporization.

Combining these three requirements for each wavelength yields a roughly triangular-shaped region of parameter space for which tissue is removed with minimal collateral damage. For a given pulse width, the superpulse intensity must exceed the thresholds defined by the energy and power density requirements for explosive vaporization. Minimization of collateral damage then sets an upper limit on the superpulse intensity. The hatched regions of superpulse intensity and pulse width shown in Fig. 2 define wavelength-dependent 'sweet-spots' for infrared tissue ablation. These limitations are in addition to those imposed by thermal confinement models (Wolbarsht, 1984). However, the thermal confinement times are long compared with the maximum pulse width in each sweet-spot, *i.e.* 5, 43 and 154 µs for 3.0, 6.1 and 6.45 µm, respectively.

The experimental parameters for previous investigations of Mark-III FEL tissue ablation have fallen within the large sweet-spot for 6.45 µm, but well outside the smaller optimal regions for 3.0 and 6.1 µm. In the original report on the preferential ablative properties of 6.45 µm radiation, various tissues were exposed to intensities of $\sim 10^{12}$ W m^{-2} and pulse widths of 2–6 µs (Edwards *et al.*, 1994). For 6.45 µm these parameters fall along the far right boundary of the sweet-spot. For 3.0 and 6.1 µm the experimental intensities were one to two orders of magnitude larger than the upper limit for minimizing collateral damage. The experimental pulse widths were also an order of magnitude outside of the sweet-spots.

Strictly interpreting these results, collateral damage could be minimized for both 3.0 and 6.1 µm by limiting the pulse widths and decreasing the superpulse intensities. However, the macroscopic ablation rates under these conditions are insufficient for surgical applications. The parameters in the upper right corner of each sweet-spot correspond to the maximum fluence per superpulse. For 3.0, 6.1 and 6.45 µm the maximum fluences within the sweet-spot are 8, 16 and 3×10^{5} kJ m^{-2}, respectively. In general, the macroscopic ablation rate is proportional to the average incident intensity. Thus, for similar superpulse repetition rates the maximum macroscopic ablation rate consistent with minimal collateral damage would be four orders of magnitude greater at 6.45 µm than at either 3.0 or 6.1 µm. In previous experiments the superpulse fluence of the Mark-III FEL was only $\sim 4 \times 10^{3}$ kJ m^{-2} (Edwards *et al.*, 1994). Even so, to match the 30 Hz performance of a Mark-III FEL at 6.45 µm, in terms of ablation rate and collateral damage, an idealized laser system at 3.0 µm would need a pulse repetition rate of $\sim$15 kHz.

These model calculations help to explain the preferential ablative properties of a Mark-III FEL tuned to 6.45 µm. As important, they detail the optimal design parameters for a dedicated 6.45 µm surgical laser system. While a Mark-III FEL has been used successfully in human surgeries on brain tumors (Copeland *et al.*, 1998, 2000) and the optic nerve (Joos *et al.*, 2000), its use is limited by the small number of infrared FEL facilities. A dedicated 6.45 µm surgical laser system would make this technology a more viable option for medical practitioners. To maximize the effectiveness of a dedicated laser system, the design goals should correspond to the maximum per pulse fluence consistent with minimal collateral damage. To this end, one should recognize that the sweet-spot boundaries given in Fig. 2 are only a rough guide. Although the wavelength-dependence shown in Fig. 2 is striking, substantial uncertainties exist in our threshold estimates for individual wavelengths. Factors contributing to this uncertainty include the high-temperature rates of protein denaturation (Kampmeier *et al.*, 2000), the heterogeneous nucleating density of soft tissues (Skripov, 1988; Venugopalan *et al.*, 1996) and the generalization of our laminar model to other tissues. Nonetheless, for typical focused spot sizes of diameter 100 µm, the upper right corner of the 6.45 µm sweet-spot corresponds to a maximum pulse width of

10 µs and a maximum energy of 2.4 J per pulse. A Mark-III FEL can achieve sufficient ablation rates at superpulse energies $100\times$ less than this maximum (Edwards *et al.*, 1994). Thus, a dedicated 6.45 µm surgical laser system should produce pulses that are several microseconds long, with 10–50 mJ or more per pulse at a repetition rate of at least 10 Hz. Like the Mark-III FEL, a dedicated laser system could have substructure to these pulses, but picosecond pulses are not necessary.

References

Colson, W. B., Johnson, E. D., Kelley, M. J. & Schwettman, H. A. (2002). *Phys. Today*, p. 35.

Copeland, M. L., Cram, G. P., Edwards, G. S., Ernst, D., Gabella, W. & Jansen, D. (2000). Presented at *SPIE International Biomedical Optics Symposium*. San Jose, CA, USA.

Copeland, M. L., Maciunas, R. J. & Edwards, G. S. (1998). In *Neurosurgical Topics: Advanced Techniques in Central Nervous System Metastases*, ch. 7, edited by R. J. Maciunas. Park Ridge, IL: The American Association of Neurological Surgeons.

Davson, H. (1972). *The Physiology of the Eye*. New York: Academic Press.

Edwards, G., Hutson, M. S. & Hauger, S. A. (2002). *Proc. SPIE*, **4633**, 184–193.

Edwards, G., Logan, R., Copeland, M., Reinisch, L., Davidson, J., Johnson, J. B., Maciunas, R., Mendenhall, M., Ossoff, R., Tribble, J., Werkhaven, J. & O'Day, D. (1994). *Nature (London)*, **371**, 416–419.

Hale, G. M. & Querry, M. R. (1973). *Appl. Opt.* **12**, 555–563.

Hutson, M. S., Hauger, S. A. & Edwards, G. (2002). *Phys. Rev. E*, **65**, 061906.

Joos, K. M., Shen, J. H., Shetlar, D. J. & Casagrande, V. A. (2000). *Lasers Surg. Med.* **27**, 191–205.

Kampmeier, J., Radt, B., Birngruber, R. & Brinkmann, R. (2000). *Cornea*, **19**, 355–363.

Landau, L. d. & Liftshitz, E. M. (1987). *Fluid Mechanics*, 2nd ed. Oxford: Pergamon Press.

Madey, J. M. J. (1971). *J. Appl. Phys.* **42**, 1906.

Skripov, V. P. (1988). *Thermophysical Properties of Liquids in the Metastable (Superheated) State*. New York: Gordon & Breach.

Venugopalan, V., Nishioka, N. S. & Mikic, B. B. (1996). *Biophys. J.* **70**, 2981–2993.

Wolbarsht, M. L. (1984). *IEEE J. Quant. Electron.* **20**, 1427–1432.